Accurate electron affinity of V and fine-structure splittings of V^- via slow-electron velocity-map imaging

Xiaoxi Fu, Zhihong Luo, Xiaolin Chen, Jiaming Li, and Chuangang Ning

Citation: The Journal of Chemical Physics **145**, 164307 (2016);
View online: https://doi.org/10.1063/1.4965928
View Table of Contents: http://aip.scitation.org/toc/jcp/145/16
Published by the American Institute of Physics

Accurate electron affinity of V and fine-structure splittings of V^- via slow-electron velocity-map imaging

Xiaoxi Fu,[1] Zhihong Luo,[1,a)] Xiaolin Chen,[1] Jiaming Li,[1] and Chuangang Ning[1,2,a)]
[1]*Department of Physics, State Key Laboratory of Low-Dimensional Quantum Physics, Tsinghua University, Beijing 10084, China*
[2]*Collaborative Innovation Center of Quantum Matter, Beijing, China*

(Received 1 September 2016; accepted 10 October 2016; published online 27 October 2016)

We report the high-resolution photoelectron spectra of negative vanadium ions obtained via the slow-electron velocity-map imaging method. The electron affinity of V was determined to be 4255.9(18) cm^{-1} or 0.527 66(20) eV. The accuracy was improved by a factor of 60 with regard to the previous measurement. The fine structure of V^- was well resolved: 35.9(11) ($^5D_1$), 103.8(12) ($^5D_2$), 204.17(74) ($^5D_3$), and 330.58(40) cm^{-1} ($^5D_4$) above the ground state $^5D_0$, respectively. *Published by AIP Publishing.* [http://dx.doi.org/10.1063/1.4965928]

I. INTRODUCTION

Electron affinity (EA), defined as the energy released when an electron is added into a neutral atom, reflects the ability of an atom to accept an electron. It helps the understanding of atomic structure and reactivity. Moreover, EA provides key parameters in determining gas phase acidities and bond dissociation energies with respect to the thermodynamic field. With the development of the measurement methods and the narrow-width lasers, the accuracy of the measured EAs of many elements has been improved steadily during the past four decades.[1–3] However, uncertainties of EA values for many transition metals still remain 10 meV.[4,5] This is mainly due to the limited energy resolution of the generic laser photoelectron spectroscopy (LPES).[6–9] Most of EA values of transition metals were measured via this method by Lineberger and co-workers in 1981.[6]

Another method established in 1970 called laser photodetachment threshold (LPT) also has measured EA values of many elements.[4,10–16] LPT method relies on the Wigner threshold law.[17] The photodetachment cross section is proportional to $E_k^{(l+1)/2}$ for a threshold photodetachment. Here, l is the angular-momentum quantum number of the photoelectron after the detachment, and E_k is the kinetic energy of the photoelectron. As a result, the sharp onset of the cross section for an s-wave photodetachment near the threshold can yield a very accurate EA value. However, the zero-slope onset for a p-wave threshold photodetachment leads to an ambiguity in determining the EA value. Moreover, the LPT method cannot resolve the congested p-wave photodetachment channels either. Unfortunately, the ability to resolve many congested p-wave channels is indispensable to measure the electron affinities of transition elements due to their unique electronic configurations. Therefore, the LPT method is mainly used for the EA measurement of main group elements. Only a few EA values of the late transition metals were measured using the LPT method, such as Ni, Pd, and Ru.[15,18]

Recently, Blondel and co-workers developed a new method known as laser photodetachment microscopy (LPM). It reduced the uncertainties of O^- and Se^- down to 1 μeV.[19,20] In view of the fact that the energy of photoelectrons is obtained through the interference patterns, the typical E_k of photoelectrons for LPM has to be lower than 1 cm^{-1}, which will lead to an unpractical lower count rate for a p-wave photodetachment. In the present work, we employed the slow-electron velocity-map imaging (SEVI) technique to conduct the precise measurement of the EA value of V and the fine-structure splittings of V^-. SEVI was originally introduced by Neumark and co-workers for improving the energy resolution of photoelectron spectroscopy of molecular anions.[21,22] Compared with the generic LPES, SEVI has an impressive energy resolution for low-energy electrons. The energy resolution of a few cm^{-1} is readily available.[23–28] In contrast to the measurement just above the threshold for LPT and LPM, SEVI usually measures the photoelectrons with $E_k \sim 100$ cm^{-1}. Therefore, SEVI can significantly improve the signal intensity.

In our previous work, we have successfully determined the EA value of Nb as 0.917 40 (6) eV using the SEVI method.[24] In the present work, we aim to improve the accuracy of EA(V) and the fine structure of V^- via the SEVI method. The ground-state configuration of V^- is $(3d^4 4s^2)$ $^5D_0$, while the ground-state configuration of V is $(3d^3 4s^2)$ $^4F_{3/2}$. Utilizing LPES method combined with a fixed frequency 488-nm laser, Lineberger and co-worker measured the EA value of V to be 0.526(12) eV.[6] Vanadium is the common constituents in production of steel alloys because vanadium can considerably increase the strength of steel. As far as the vanadium oxide is concerned, V_2O_5 is widely used as a catalyst in manufacturing industries. Moreover, the vanadium redox batteries are currently used for the grid energy storage.[29]

II. EXPERIMENTAL METHODS

Fig. 1 shows the schematic diagram of the experimental apparatus used in the present work. The whole apparatus can

a)Electronic addresses: luozhihong@mail.tsinghua.edu.cn and ningcg@tsinghua.edu.cn

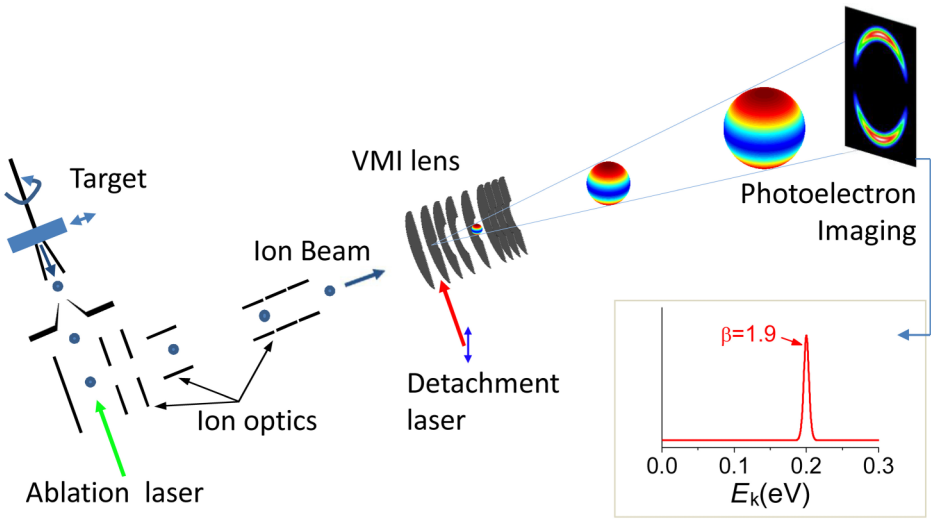

FIG. 1. Schematic diagram of the experimental setup. A mass gate and a rotatable ion detector in the front of the VMI lens are not shown. The inset in the lower right corner shows the photoelectron spectrum reconstructed from the projected image. See text for details.

be divided into three main parts: a laser ablation ion source, a Wiley-McLaren type time-of-flight (TOF) mass spectrometer, and a photoelectron velocity-map imaging (VMI) system. The negative ion V^- is generated via a pulsed laser ablation ion source. The second-harmonic output of a Nd:YAG laser (532 nm) (20 Hz, ~15 mJ/pulse) is focused onto a continually rotating as well as translating V metal disk. An in-line sodium oven is applied to release the sodium vapor so as to remove the trace oxygen and water contamination in the source cell. Otherwise, the dominant species are the anions of vanadium oxides. After the skimmer, the anionic species are extracted perpendicularly by a −900 V high-voltage plates. Then, the ion beam is guided by a set of deflectors and focused into a 1.4-m-long TOF tube. The mass resolution (M/ΔM) of the current design is 300 for M ~ 100. Then the target anions are picked out by the mass gate and detected by an in-line microchannel plate detector. The ion detector is rotatable and can be moved out of the ion path if the subsequent photoelectron imaging is underway. The velocity-map imaging (VMI) lens system is similar to the design from Ref. 30, which was originally used by the ion imaging experiment.[31,32] Afterwards, the selected anions enter the VMI lens system through a 6-mm-diameter aperture on the repeller plate and are perpendicularly crossed by the detachment laser beam. Finally, the detached photoelectrons are projected onto a phosphor screen behind a set of microchannel plates and recorded by a CCD camera. A real-time intensity-weighted centroid program is applied to determine the hitting position of each photoelectron. Typically, each photoelectron imaging is an accumulated result of 50 000–300 000 laser shots. The photodetachment laser is from a Spectra-physics dye laser system (400-920 nm, line width 0.06 cm^{-1} at 625 nm) pumped by a Quanta-Ray Pro 290 Nd:YAG laser (20 Hz, 1000 mJ/pulse at 1064 nm). The detachment laser is linearly polarized. The polarization direction is parallel to the phosphor screen. Since the photoelectron distribution has a cylindrical symmetry, the photoelectron spectrum and the angular distribution can be reconstructed from the projected image without losing information. In the present work, we use the maximum entropy velocity Legendre reconstruction (MEVELER) method for the reconstruction.[33] For one-photon detachment with linearly polarized light, the photoelectron angular distribution is described by[34]

$$\frac{d\sigma}{d\Omega} = \frac{\sigma_{total}}{4\pi}\left[1 + \beta P_2(\cos\theta)\right]. \quad (1)$$

Here θ is the outgoing direction of the photoelectron relative to the polarization axis of the laser, σ_{total} is the total photodetachment cross section, β is the asymmetry parameter, and P_2 is the second order Legendre polynomial. The value of β ranges from −1 to 2. It depends on the electronic state and the kinetic energy of the photoelectrons. For a positive asymmetry parameter β, the intensity of photoelectrons along the direction parallel to the polarization axis is higher than that along the perpendicular direction. For example, the photodetachment of an s-subshell electron yields a p-wave and will generate a positive β. This is the case for the present EA measurement of V. While for a negative β, the photoelectron intensity perpendicular to the polarization axis is higher, which is usually due to the interference of the different partial waves of outgoing photoelectrons. The photon energy ($h\nu$) is further measured by a HighFinesse WS6-600 wavelength meter with an accuracy of 0.02 cm^{-1}.

III. RESULTS AND DISCUSSION

Fig. 2 shows the photoelectron images and binding energy spectra obtained at photo energy $h\nu$ = 12 647.43, 12 700.42, and 12 811.79 cm^{-1}, respectively. The imaging voltage is −150 V. Each photoelectron image is obtained with 300 000 laser shots. The photoelectron angular distributions clearly show a parallel transition, which are consistent with the expected p-wave detachment. At $h\nu$ = 12 811.79 cm^{-1}, the asymmetry parameter β for the peak a + b + c + d is 2.00. The values of β are 1.93, 1.92, and 1.85 for peaks e, f, and g, respectively. The uncertainties are estimated as 0.10. The β value of the weak peak h is 0.99 with an

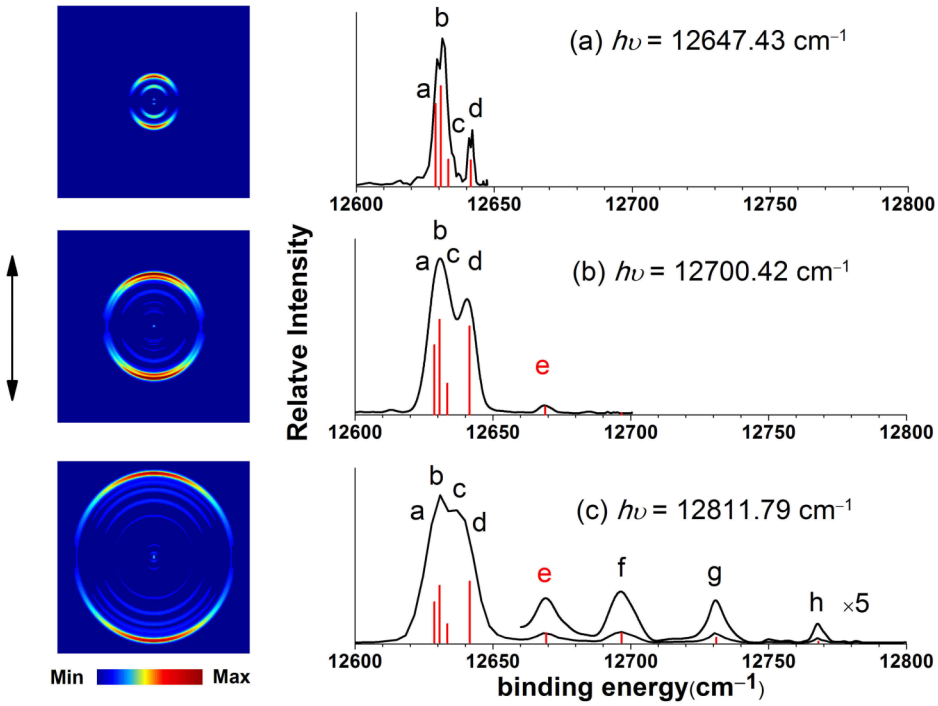

FIG. 2. Photoelectron images and spectra of V^- ions at photon energies of 12 647.43 cm^{-1} (a), 12 700.42 cm^{-1} (b), and 12 811.79 cm^{-1} (c). The double arrow indicates the laser polarization. The red sticks are the theoretical simulations at the ion temperature 800 K. Peak *e* is related to the V ($^4D_{1/2}$) ← V^- ($^5D_0$) transition, which is used to measure the electron affinity of V in the present work. The heights of the weak peaks e–h were multiplied by 5 for a better view in the panel (c).

uncertainty 0.24. According to the transition rules, there are eight allowed transitions between V^- (^5D) and V (^4D), which are labeled as *a*-*h* in Fig. 2. The diagram of the transitions is illustrated in Fig. 3. There are five peaks in Fig. 2(c). The first broad peak includes four transitions a, b, c, and d according to the theoretical simulation. Peak e is related to the transition V^- ($^5D_0$) ← V ($^4D_{1/2}$). This is the sole channel from the ground state of V^-. Therefore, the transition V^- ($^5D_0$) ← V ($^4D_{1/2}$) is used to measure the EA value of V in the present work. Peak f is related to the transition V^- ($^5D_1$) ← V ($^4D_{3/2}$). Since the energy levels of V ($^4D_{1/2}$) and V ($^4D_{3/2}$) are accurately known according to the NIST database,[35] the energy gap between V^- ($^5D_0$) and V^- ($^5D_1$) can be obtained from peaks e and f. Peaks g and h are related to transitions V^- ($^5D_2$) ← V ($^4D_{5/2}$) and V^- ($^5D_3$) ← V ($^4D_{7/2}$), respectively. Similarly, the energy levels of V^- ($^5D_2$) and V^- ($^5D_3$) can be determined from peaks g and h. To determine the energy level of V^- ($^5D_4$), we need a better energy resolution to resolve the overlapped transitions a, b, c, and d. One important feature of SEVI is that its energy resolution can be improved by lowering the kinetic energy of photoelectrons. As shown in Figs. 2(b) and 2(a), peak d is well resolved from other peaks at lower photon energies $h\upsilon$ = 12 700.42 and 12 647.43 cm^{-1}. Once the binding energy of peak d is measured, the energy level of V^- ($^5D_4$) can be determined although peaks a, b, and c still overlap. The binding energies of peaks a, b, and c can be derived indirectly because the energy levels of neutral V atoms are accurately known.[35] The binding energies of all peaks and the energy levels of all related states are summarized in Table I and Fig. 3. The obtained binding energy difference between peaks a and b is 1.9 cm^{-1}, and the binding energy difference between peaks b and c is 2.8 cm^{-1}. In principle, it is possible to resolve peaks a, b, and c by further lowering the photon energy. However, the photoelectron intensity becomes extremely weak due to the Wigner threshold law. The precision cannot be improved by lowering the photon energy further due to the poor signal-to-noise ratio. The red sticks in Fig. 2 indicate the calculated intensity of each assigned transition, which is derived from the assumption of L-S coupling and is rescaled by the Wigner's law at the ion temperature of 800 K. It can be seen that the simulation agrees well with the experimental spectra.

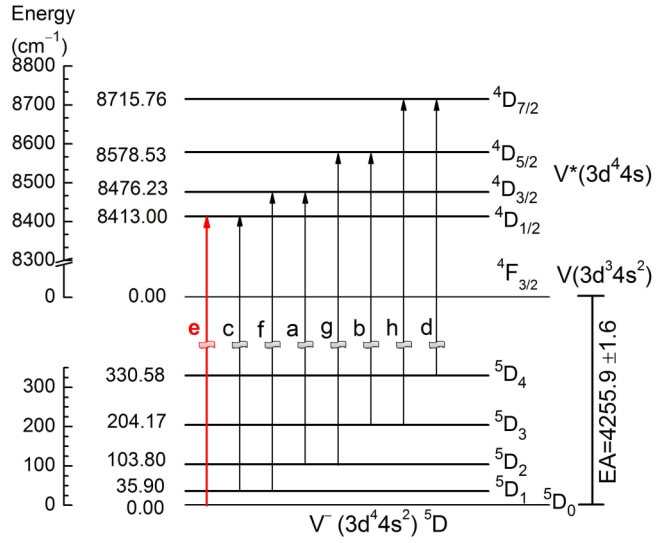

FIG. 3. Energy levels of V and V^- related to the present measurement. The ground state of V is $^4F_{3/2}$. The ground state of V^- is $^5D_0$. The labels of each transition are the indexes of the observed peaks in Fig. 2. The transition *e* is used for the electron-affinity measurement.

To accurately determine the electron affinity of V, the binding energy of peak e [V^- ($^5D_0$) ← V ($^4D_{1/2}$)] was measured around its threshold further. A fine energy calibration of the VMI system for peak e was done by

TABLE I. Measured binding energies and fine structures of V^- and the electron affinity of V.

Peaks	Levels ($V \leftarrow V^-$)	Binding energy (cm^{-1})
a	$^5D_2 \leftarrow {}^4D_{3/2}$	12 628.7(12)[a]
b	$^5D_3 \leftarrow {}^4D_{5/2}$	12 630.6(8)[a]
c	$^5D_1 \leftarrow {}^4D_{1/2}$	12 633.4(18)[a]
d	$^5D_4 \leftarrow {}^4D_{7/2}$	12 641.5(2)
e	$^5\mathbf{D}_0 \leftarrow {}^4\mathbf{D}_{1/2}$	**12 668.9(16)**[b]
f	$^5D_1 \leftarrow {}^4D_{3/2}$	12 696.7(18)
g	$^5D_2 \leftarrow {}^4D_{5/2}$	12 731.0 (12)
h	$^5D_3 \leftarrow {}^4D_{7/2}$	12 767.9(8)

Fine structures of V^- (cm^{-1})

Levels	Extrapolated[5]	Experimental
$^5D_1 \leftarrow {}^5D_0$	35(4)	35.9(11)
$^5D_2 \leftarrow {}^5D_0$	105(8)	103.8(12)
$^5D_3 \leftarrow {}^5D_0$	205(13)	204.17(74)
$^5D_4 \leftarrow {}^5D_0$	330(17)	330.58(40)

Electron affinity of V

Value	Reference
1.74 eV	Cole and Perdew[37] (calculated)
0.530 eV	Balabanov and Peterson[38] (calculated)
0.526(12) eV	Feigerle *et al.*[6] (measured)
0.527 66(20) eV or 4255.9(16) cm^{-1}	This work (measured)

[a]These values are extracted by using the energy intervals of V^- and the related measured transitions.
[b]The selected transition for the EA measurement.

scanning the photon energy from 12 700 cm^{-1} to 12 810 cm^{-1} with a ~20-cm^{-1} step. The kinetic energy of photoelectrons E_k is proportional to the radius squared r^2 of the photoelectron image. $h\nu$ is monitored by a wavelength meter with an accuracy 0.02 cm^{-1}, and r is obtained via SEVI. The measured r^2 versus the photo energy $h\nu$ is plotted in Fig. 4. The binding energy of the transition e and its uncertainty were determined by a best linear fitting. Fig. 5 shows the binding energy of peak e versus the photo electron kinetic energy. The mean binding energy is 12 668.9 cm^{-1} with an

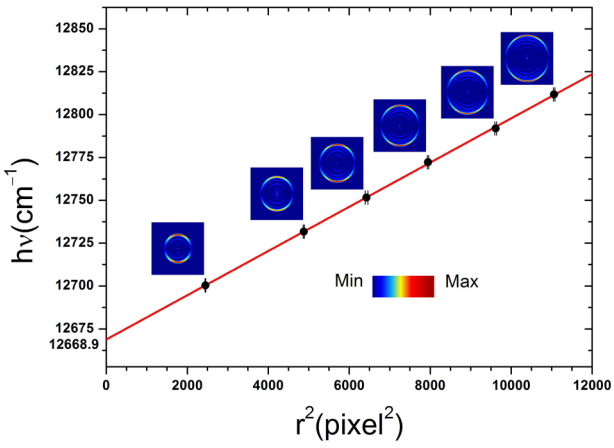

FIG. 4. The radius squared r^2 of the photoelectron image for the transition e [V ($^4D_{1/2}$) ← V^- ($^5D_0$)] versus the photon energy $h\nu$. The solid line is the best linear fitting. The intercept 12 668.9 cm^{-1} is the binding energy of the transition e. The rings above each point are the photoelectron images.

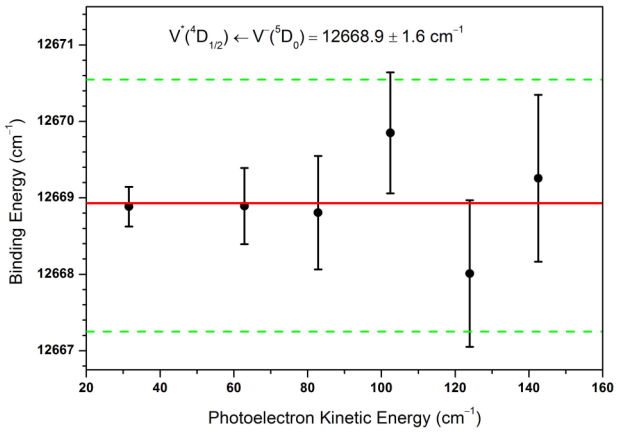

FIG. 5. Binding energy of V ($^4D_{1/2}$) ← V^- ($^5D_0$) transition measured as a function of the photoelectron kinetic energy. The dotted lines indicate the ±1.6 cm^{-1} uncertainty.

uncertainty of 1.6 cm^{-1}. The uncertainty is mainly caused by the influence of the strong peak a + b + c + d, as shown in Fig. 2(b). The uncertainty of 1.6 cm^{-1} has included the contribution of the laser linewidth 0.06 cm^{-1}. The energy level of the neutral V atom ($3d^4 4s$) $^4D_{1/2}$ is 8413.00 cm^{-1} above its ground state. Subtracting 8413.00 cm^{-1} from the binding energy 12 668.9 cm^{-1} yields the EA value of V: 4255.9(16) cm^{-1} or 0.527 66(20) eV, which is consistent with the previously reported value of 0.526(12) eV.[6] The accuracy has been improved by a factor of 60. Note that 1 eV = 8065.544 005(50) cm^{-1}, as recommended by 2014 CODATA.[36] The fine-structure splittings of V^- are determined to be 35.9(11) ($^5D_1$), 103.8(12) ($^5D_2$), 204.17(74) ($^5D_3$), and 330.58(40) cm^{-1} ($^5D_4$) above the ground state $^5D_0$, respectively. In Table I, the previous extrapolated values of the splittings 35(4), 105(8), 205(13), and 330(17) cm^{-1} are also listed for comparison.[6] The extrapolated values agree with our measurement very well. The typical error is only ~1 cm^{-1}. With regard to theoretical side, the early calculation suggested EA(V) to be 1.74 eV.[37] A more recent calculation reported a value of 0.530 eV.[38] The accurate experimental EA(V) value measured in this work could serve as a reliable benchmark for developing more advanced theoretical calculations for transition metals.

IV. CONCLUSIONS

In summary, the electron affinity of V was measured to be 4255.9(18) cm^{-1} or 0.527 66(20) eV. The accuracy was improved by a factor of 60 with respect to the previous measurement. The fine-structure of V^- was also precisely measured. The success mainly thanks to the unique features of the slow-electron velocity-map imaging method. On one hand, it involves the well-above-threshold measurement immune to the low p-wave signal intensity at the threshold. On the other hand, its high energy resolution can resolve the congested p-wave channels. The accurate value of the electron affinity of V and the fine-structure splittings of V^- determined in this study could serve as a benchmark for developing more accurate theoretical methods for transition metals.

ACKNOWLEDGMENTS

This work is supported by National Natural Science Foundation of China (NSFC) (Grant Nos. 91336104 and 11504198) and Ministry of Science and Technology of China (MOST) (Grant No. 2013CB922004) of the National Key Basic Research Program of China. Z.H.L. thanks China Postdoctoral Science Foundation funded project (Grant No. 2015M580081).

[1]W. C. Lineberger, Annu. Rev. Phys. Chem. **64**, 21 (2013).
[2]T. Andersen, Phys. Rep. **394**, 157 (2004).
[3]W. C. Lineberger and B. W. Woodward, Phys. Rev. Lett. **25**, 424 (1970).
[4]H. Hotop and W. C. Lineberger, J. Phys. Chem. Ref. Data **14**, 731 (1985).
[5]J. C. Rienstra-Kiracofe, G. S. Tschumper, H. F. Schaefer III, S. Nandi, and G. B. Ellison, Chem. Rev. **102**, 231 (2002).
[6]C. S. Feigerle, R. R. Corderman, S. V. Bobashev, and W. C. Lineberger, J. Chem. Phys. **74**, 1580 (1981).
[7]V. T. Davis, J. Thompson, and A. Covington, Nucl. Instrum. Methods Phys. Res., Sect. B **241**, 118 (2005).
[8]J. Felton, M. Ray, and C. C. Jarrold, Phys. Rev. A **89**, 033407 (2014).
[9]D. G. Leopold and W. C. Lineberger, J. Chem. Phys. **85**, 51 (1986).
[10]M. Scheer, R. C. Bilodeau, and H. K. Haugen, Phys. Rev. Lett. **80**, 2562 (1998).
[11]D. M. Neumark, K. R. Lykke, T. Andersen, and W. C. Lineberger, Phys. Rev. A **32**, 1890 (1985).
[12]R. C. Bilodeau, M. Scheer, and H. K. Haugen, J. Phys. B: At., Mol. Opt. Phys. **31**, 3885 (1998).
[13]M. Scheer, R. C. Bilodeau, C. A. Brodie, and H. K. Haugen, Phys. Rev. A **58**, 2844 (1998).
[14]R. C. Bilodeau, M. Scheer, H. K. Haugen, and R. L. Brooks, Phys. Rev. A **61**, 012505 (1999).
[15]M. Scheer, C. A. Brodie, R. C. Bilodeau, and H. K. Haugen, Phys. Rev. A **58**, 2051 (1998).
[16]R. C. Bilodeau and H. K. Haugen, Phys. Rev. Lett. **85**, 534 (2000).
[17]E. P. Wigner, Phys. Rev. **73**, 1002 (1948).
[18]P. L. Norquist, D. R. Beck, R. C. Bilodeau, M. Scheer, R. A. Srawley, and H. K. Haugen, Phys. Rev. A **59**, 1896 (1998).
[19]C. Blondel, C. Delsart, C. Valli, S. Yiou, M. R. Godefroid, and S. Van Eck, Phys. Rev. A **64**, 052504 (2001).
[20]M. Vandevraye, C. Drag, and C. Blondel, Phys. Rev. A **85**, 015401 (2012).
[21]A. Osterwalder, M. J. Nee, J. Zhou, and D. M. Neumark, J. Chem. Phys. **121**, 6317 (2004).
[22]D. M. Neumark, J. Phys. Chem. A **112**, 13287 (2008).
[23]J. B. Kim, J. A. DeVine, D. S. Levine, and D. M. Neumark, J. Am. Chem. Soc. **137**, 1420 (2015).
[24]Z. H. Luo, X. L. Chen, J. M. Li, and C. G. Ning, Phys. Rev. A **93**, 020501(R) (2016).
[25]X. L. Chen, Z. H. Luo, J. M. Li, and C. G. Ning, Sci. Rep. **6**, 24996 (2016).
[26]J. B. Kim, M. L. Weichman, T. F. Sjorlander, D. M. Neumark, J. Klos, M. H. Alexander, and D. E. Manolopoulos, Science **349**, 510 (2015).
[27]H. T. Liu, C. G. Ning, D. L. Huang, P. D. Dau, and L. S. Wang, Angew. Chem., Int. Ed. **53**, 2464 (2014).
[28]H. T. Liu, C. G. Ning, D. L. Huang, and L. S. Wang, Angew. Chem., Int. Ed. **52**, 8976 (2013).
[29]L. Joerissen, J. Garche, C. Fabjan, and G. Tomazic, J. Power Sources **127**, 98–104 (2004).
[30]I. Leon, Z. Yang, H. T. Liu, and L. S. Wang, Rev. Sci. Instrum. **85**, 083106 (2014).
[31]W. Li, S. D. Chambreau, S. A. Lahankar, and A. G. Suits, Rev. Sci. Instrum. **76**, 063106 (2005).
[32]A. T. J. B. Eppink and D. H. Parker, Rev. Sci. Instrum. **68**, 3477 (1997).
[33]B. Dick, Phys. Chem. Chem. Phys. **16**, 570–580 (2014).
[34]J. Cooper and R. N. Zare, J. Chem. Phys. **48**, 942 (1968).
[35]J. E. Sansonetti and W. C. Martin, J. Phys. Chem. Ref. Data **34**, 1559 (2005).
[36]P. J. Mohr, D. B. Newell, and B. N. Taylor, Rev. Mod. Phys. **88**, 035009 (2016).
[37]L. A. Cole and J. P. Perdew, Phys. Rev. A **25**, 1265 (1982).
[38]N. B. Balabanova and K. A. Peterson, J. Chem. Phys. **125**, 074110 (2006).